Journal of Materials Chemistry A

Accepted Manuscript

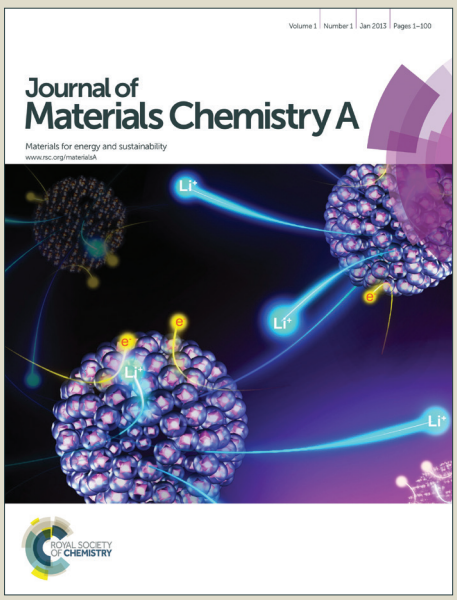

ROYAL SOCIETY OF CHEMISTRY

www.rsc.org/materialsA

Gold-palladium bimetallic nanoalloys decorated ultrathin 2D TiO_2 nanosheets as efficient photocatalysts with highly hydrogen evolution activity

Yongji Xin [a,b], Linen Wu [b], Lei Ge* [a, b], Changcun Han [b], Yujing Li [b], Siman Fang [b]

[a] State Key Laboratory of Heavy Oil Processing, College of Science, China University of Petroleum Beijing, No. 18 Fuxue Rd., Beijing 102249, People's Republic of China.

[b] Department of Materials Science and Engineering, College of Science, China University of Petroleum Beijing, No. 18 Fuxue Rd., Beijing 102249, People's Republic of China.

Abstract

In this work, a novel AuPd bimetallic nanoalloys decorated ultrathin 2D titanium dioxide (TiO_2) nanosheets with highly active H_2 evolution activity was prepared via a facile in situ synthesis method. The physical and photophysical properties of the as-prepared AuPd/TiO_2 nanosheets were characterized by X-ray diffraction (XRD), transmission electron microscope (TEM), UV-visible diffuse reflection spectroscopy (DRS), X-ray photoelectron spectroscopy (XPS), electron spin resonance (ESR) and surface photocurrent spectroscopy (SPC). The photocatalytic H_2 evolution experiments indicate that the AuPd co-catalysts can efficiently promote the separation of photogenerated charge carriers in TiO_2, and consequently enhance the H_2 evolution activity. The 0.3 wt% AuPd/TiO_2 sample shows the highest catalytic activity, and corresponding H_2 evolution rate is 526 μmol h^{-1} g^{-1}, which is enhanced by 31 times higher than that of pure TiO_2 under simulated sunlight (λ>300 nm) irradiation. A possible mechanism of the enhanced simulated sunlight catalytic performance of AuPd bimetallic nanoparticles (NPs) decorated TiO_2 nanosheets is proposed to guide further improvement of desirable functional materials. It is expected that the AuPd decorated TiO_2 nanosheets obtained via sample synthesis approach can be used as efficient photocatalysts and provide promising potentials for new energy applications.

Keywords: AuPd bimetallic nanoalloys; TiO_2 nanosheets; Photocatalysis; Hydrogen evolution.

1. Introduction

Metal oxide semiconductor-mediated photocatalysis has attracted worldwide attention due to its potential in environmental and energy-related applications.[1-4] Among various semiconductor photocatalysts, titanium doxide (TiO_2) is considered as one of the most promising photocatalysts in water splitting,[5-7] water cleaning[8,9] and air purification[10,11] owing to its excellent photocatalytic properties, high stability, low cost and nontoxicity. However, the light response range and the catalytic activity of TiO_2 are limited due to its large band gap (3.2 eV), high recombination rate of photo-excited charge carriers and low separation efficiency.

Many attempts have been made to improve the photocatalytic performance of TiO_2, such as noble metal deposition (Au, Pt),[12,13] nonmetal doping (CdS, Sr^{2+}),[14-16] semiconductor hetero-junction modification (such as g-C_3N_4, Ag_3PO_4, WO_3, et al)[17-19] and design of black hydrogenated TiO_2,[20] red and blue TiO_2 sample,[21] TiO_2 nanosheets.[22,23] Among various strategies, the rapid separation-transfer-transformation of photo-generated charge carriers is a critical issue. For instance, noble metallic nanoparticles have been widely investigated as co-catalysts. In particular, bimetallic nanoparticles (NPs) in the form of either alloys or core-shell nanostructures attract great interest from both scientific and technological perspectives for their improved catalytic properties, resulting from not only size effect but also the combination of different metals.[24,25] It is observed that the activity, selectivity and resistance to poisoning of the metal catalysts can be drastically influenced by the presence of a second metal component.[26] Various bimetallic alloy NPs with improved performance have been reported, such as PtAu, PtNi, AuCu and PtSn et al.[27-30] Furthermore, recent studies have shown superior activities of supported alloyed gold-palladium (AuPd) catalysts in different types of reactions

such as in the hydrodechlorination of chlorofluorocarbons (CFCs), in the hydridesulphurisation reaction, in the direct peroxide formation from H_2/O_2 mixtures.[31-34] Despite these success reports, the use of bimetallic AuPd alloys for photocatalytic water splitting has still limited. Thus, it should be of great interest to design bimetallic alloys decorated photocatalysts with significantly enhanced activities, which will enrich the catalytic chemistry and extend their applications in environmental protection fields.

In this study, for the first time we report the synthesis of bimetallic AuPd decorated ultrathin 2D TiO_2 nanosheets via in situ synthesis method and the applications in photocatalytic H_2 evolution under UV-visible light irradiation. The activity of TiO_2 nanosheets can be significantly improved after introducing the mono-disperse AuPd bimetallic NPs. The 0.3 wt% AuPd/TiO_2 shows the highest H_2 evolution activity of 526 μmol h^{-1} g^{-1}, which is enhanced by 31 times higher than that of pure TiO_2 nanosheets under the same conditions. The effects of AuPd alloy NPs contents on the light absorption, charge transfer process and photocatalytic activity were investigated in detail, and the photocatalytic mechanism for enhanced H_2 evolution activity was also discussed. The work may provide new insight into synthesizing novel hybrid photocatalytic materials with potential applications in solar energy conversion and utilization.

2. Experimental

2.1. Materials

Titanium isopropoxide (TTIP, Aladdin, 95%), concentrated HCl solution (37%), ethyl alcohol (EtOH, A.R.), polyethylene oxide-polypropylene oxide–polyethylene oxide (PEO20–PPO70–PEO20, Pluronic P123), $HAuCl_4 \cdot 3H_2O$ (1g, A.R.), $PdCl_2$ (1g, A.R.), poly vinyl alcohol (PVA, Aldrich, MW=10000, 80% hydrolyzed), ethylene glycol (EG) and $NaBH_4$ (Aladdin, 98%) were used as received without additional purification or treatment. Deionized water was used as the solvent for all of the

solutions or dispersions.

2.2. Synthesis of the photocatalysts

The ultrathin 2D TiO_2 nanosheets was prepared according to a literature method with a slight modification.[35] 1.05 g TTIP was added into 0.74 g concentrated HCl solution during vigorous stirring solution A); and 0.2 g Pluronic P123 was dissolved in 3.0 g ethanol (solution B). After stirring for 15 min, the solution B was added into solution A and stirred for another 30 min. Then, 2.5 ml TTIP solution with 20 ml EG was transferred into a 50 ml autoclave and heated at 150 ^oC for 40 h. The products of the hydrothermal reaction were washed with ethanol three times, and the white powders were collected after washing/centrifugation and drying at 80 ^oC for 24 h.

The preparation of AuPd/TiO_2 nanosheets composite photocatalysts is described as follows:[36] in a typical procedure, 1 mM $HAuCl_4 \cdot 3H_2O$ and $PdCl_2$ aqueous solution were first prepared. Fresh aqueous solutions of 0.1 M $NaBH_4$ and PVA were also prepared in advance. The as prepared TiO_2 nanosheets (0.1 g) was added to beaker containing 100 mL deionized water, and then sonicated for 30 min. The $PdCl_2$ (1 mM) and $HAuCl_4$ (1 mM) stock solutions mixed in the desired ratio ((Au/Pd) (wt/wt) = 1) and the required amount (1.0 wt%) of a PVA solution ware added (PVA/(Au + Pd) (wt/wt) = 1.2) into the as prepared TiO_2 nanosheets aqueous solution; After stirring for 15 min, the freshly prepared solution of $NaBH_4$ ($NaBH_4$/(Au+Pd)(mol/mol)=5) was then added to the solution to form a dark-brown sol. The solution was stirred for a further 120 minutes. The product was centrifuged, washed with water and ethyl alcohol, irradiation under UV-visible light for 2 h to remove all residual organic species and then dried in a vacuum over at 80 ^oC for 24 h.

Then, AuPd/TiO_2 composites with different amounts of AuPd bimetallic alloys were obtained. The weight percentages of AuPd in the initial photocatalyst precursors were 0 wt%, 0.1 wt%, 0.3 wt%, 0.5 wt%, 1.0 wt%, respectively. As a comparison, 1.0 wt% Au/TiO_2 and 1.0 wt% Pd/TiO_2 were also

prepared.

2.3 Characterization

The crystal phase of as-prepared samples was analyzed by X-ray diffraction (XRD; Bruker D8 Advance, X-ray diffractometer) with CuKa radiation at a scan rate of 4° min^{-1}, in the 2θ range of 20°-70°. The acceleration voltage and the applied current were 40 KV and 40 mA, respectively. The morphology of the samples was examined by transmission electron microscopy (TEM, JEM-2100, accelerating voltage 200 kV) and high-resolution transmission electron microscopy (TEM, FEI Tecnai G2 F20, accelerating voltage 200 kV). UV-Vis diffuse reflection spectroscopy (DRS) was performed on a Shimadzu UV-4100 spectrophotometer using $BaSO_4$ as the reference material. The X-ray photoelectron spectroscopy (XPS) was measured in a PHI 5300 ESCA system. The beam voltage was 3.0 eV, and the energy of Ar ion beam was 1.0 keV. The binding energies were normalized to the signal for adventitious carbon at 284.6 eV. The electron spin resonance (ESR) signals of spin-trapped oxidative radicals were obtained on a Bruker model ESR JES-FA200 spectrometer equipped with a quanta-Ray Nd: YAG laser system as the light source (λ>300 nm).

2.4. SPC measurements

The surface photocurrent (SPC) measurement was carried out on a surface photocurrent spectroscopy (PL-SPS/IPCE1000 Beijing Perfect Light Technology Co., Ltd). The measurement system consists of a source of monochromatic light, a lock-in amplifier (SR830, Stanford research systems, inc.) with a light chopper (SR540, Stanford research systems, inc.), and a sample chamber. The monochromatic light is provided by passing light from a 500 W Xenon lamp (CHFXQ500 W, global Xenon lamp power) though a grating mono-chromator (Omni-5007, No.09010, Zolix), which chopped with a frequency of 30 Hz. All the measurements were operated at room temperature and under ambient pressure.

2.5. Evaluation of photocatalytic performance

The photocatalytic H_2 evolution from water splitting was carried out in a 300 ml quartz reactor at 4 ^oC. The reactor is connected to a low-temperature thermostat bath. PLS-SXE 300 UV Xe lamp (UV-visible, λ>300 nm) was used as the light source. In a typical photocatalytic experiment, 50 mg of photocatalyst powder was dispersed in a 100 ml of aqueous solution containing 25% methanol by volume. Before photocatalytic experiments, the reaction vessel was evacuated for 30 min to remove the air inside the reaction system and to ensure the anaerobic conditions. The products were analyzed by gas chromatography (Beifen 3420 A, high purity Argon as a carrier gas, 99.999%) equipped with a thermal conductivity detector.

3. Results and discussion

3.1. Characterization of AuPd/TiO_2 composite samples

The X-ray diffraction patterns of as-prepared pure TiO_2, Au/TiO_2, Pd/TiO_2, AuPd/TiO_2 photocatalysts are shown in Fig.1. Typical diffraction peaks corresponding to anatase TiO_2 (2θ=24.9°, 36.8°, 48.4°) and rutile TiO_2 (2θ=27.6°, 42.6°, 56.9°) are observed in all the samples, which are attributed to (1 0 1), (0 0 4), (2 0 0) facets of anatase TiO_2 (JCPDS, No.71-1169) and (1 1 0), (2 1 0), (2 2 0) facets of rutile TiO_2 (JCPDS, No.88-1169). It is obvious that the introducing of bimetallic AuPd species did not affect the crystal structure of ultrathin 2D TiO_2 nanosheets. Notably, no apparent peaks of AuPd were observed in all the composites. This can be ascribed to the fact that the content of AuPd is too low to be detected by XRD. However, the presence of AuPd bimetallic alloys in the composites can be easily evidenced by TEM and XPS, as discussed later.

TEM was further used to investigate the microstructures of as-prepared samples. Fig.2 illustrates TEM images (a, b, d, e) and HRTEM images (c, f) of ultrathin 2D TiO_2 nanosheets (a–c), AuPd/TiO_2 composite (d-f). As shown in Fig.2(a,b), it can be seen that the TiO_2 sample is composed of nanosheets

with their edges rolled up due to surface tension, which is similar to the general behavior of graphene. The size of the ultrathin 2D TiO_2 nanosheets is around 200 nm. Fig.2c presents the HRTEM image of ultrathin 2D TiO_2 nanosheets. The measured lattice spacings are consistent with the d-spacings of TiO_2, the lattice fringes with interplanar spacings $d_{(101)}$=0.351 nm and $d_{(004)}$=0.237 nm are consistent with the anatase phase of TiO_2 (JCPDS, No.71-1169). Fig.2(d,e) show the TEM images of AuPd/TiO_2 composite. As it can be seen, the monodisperse bimetallic AuPd NPs are deposited on the surface of ultrathin 2D TiO_2 nanosheets with high dispersion and there is no obvious change in the microstructure of ultrathin 2D TiO_2 nanosheets. Fig.2f presents the HRTEM image of AuPd/TiO_2 composite. The measured lattice spacing of 0.227 nm can be indexed to the (2 2 0) reflections of face-centered cubic (fcc) of Pd–Au alloy NPs.[37] The ultrathin 2D TiO_2 nanosheets and AuPd alloys closely combine together to form close interfaces, which is advantageous for charge transfer between the AuPd and TiO_2. As a result, it is efficient to promote the separation of photogenerated charge carriers, and then improve the photocatalytic activity.

The UV–Vis diffuse reflectance spectra was measured to determine the optical absorption properties of AuPd/TiO_2 composite samples with different AuPd NPs contents and the results were depicted in Fig.3. For the sample pure TiO_2 nanosheets, there is only strong absorbance in ultraviolet region due to the large band gap energy of TiO_2. Compared to the TiO_2 products, all the AuPd/TiO_2 samples show higher absorption capability from the UV through the visible range up to 550 nm due to the contribution of introduced dark brown AuPd bimetallic NPs and the characteristic surface plasmon resonance effect of Au species. The absorption intensity of the as-prepared samples strengthen with increasing AuPd NPs contents, which agrees with the color of the prepared samples that vary from white to dark gray. The DRS results also demonstrate that the chemical deposited AuPd bimetallic NPs have higher visible light absorption, and then have the potential to enhance photocatalytic performance.

In order to further verify the formation of bimetallic AuPd alloy NPs in the ultrathin 2D TiO_2 nanosheets, the 1.0 wt% AuPd/TiO_2 sample was examined by X-ray photoelectron spectroscopy (XPS) analysis. It has been reported that the exposed surfaces present different chemical states from the inner bulk atoms. Fig.4a and b present the high-resolution XPS spectra of O 1s and Ti 2p in the AuPd/TiO_2 sample. The binding energy of O 1s (529.6 eV) is accordance with the reference value for TiO_2.[38] The Ti $2p_{3/2}$ peak at 457.5 eV and Ti $2p_{1/2}$ peak at 463.2 eV are observed in Fig.4b. It is of interest that the core levels of Ti 2p shows a 0.5 eV shift to lower binding energy compared with the corresponding stoichiometric bulk crystals. The lower binding energy for surface atoms has been reported to be the result of electron gain (reduction) of Ti atoms from surrounding oxygen atoms, for example, from the Ti^{4+} to the Ti^{3+} state.[39] As shown in Fig.4c, the Au $4f_{7/2}$ and Au $4f_{5/2}$ peaks in the spectrum of AuPd/TiO_2 locate at 82.4 and 86.1 eV, respectively. All binding energy values of Au 4f orbital were significantly lower than that of Au/TiO_2.[40] Such a negative binding energy shift may be attributed to several factors, such as charge transfer effects from Pd or TiO_2 and the unique structure of AuPd alloys.[41] Furthermore, the Pd 3d spectra of AuPd/TiO_2 could be fitted into asymmetric peaks shown in Fig.4d, suggesting the existence of two states of Pd species. The Pd $3d_{5/2}$ peak at 334.5 eV and Pd $3d_{3/2}$ peak at 340.2 eV are attributed to the metallic Pd^0, while the binding energy peak shown at 339.2 eV is originated form of Pd^{2+} (Pd $3d_{5/2}$). The results indicated that the oxide species formed on the surface of Pd. The binding energy peaks of Pd 3d in AuPd/TiO_2 show a slight downshift compared to the peaks in the Pd/TiO_2 sample. The lower binding energy values of Pd 3d might be due to a gain of charge density in the d band, concomitant with a loss in the sp band, suggesting more Au–Pd bond formation on the surface of the AuPd NPs.

3.2. Photocatalytic H_2 evolution activity

Photocatalytic H_2-evolution activity of the as-obtained products was evaluated under UV-visible

light (λ>300 nm) irradiation in an aqueous solution containing methanol as sacrificial reagents. As shown in Fig.5, The pure TiO_2 displays a very low H_2 production rate, while all the AuPd/TiO_2 photocatalysts shows a higher rate of photocatalytic H_2-generation. Fig.6 presents the rate of H_2 evolution over AuPd/TiO_2 composite samples with different AuPd contents. After loading 0.1 wt% of AuPd NPs on the ultrathin 2D TiO_2 nanosheets, the activity of H_2 evolution is significantly increased to 249 μmol h^{-1} g^{-1}. With increase of the AuPd doping amount, the photocatalytic H_2 evolution on AuPd/TiO_2 is further enhanced. The 0.3 wt% AuPd/TiO_2 shows the highest H_2 evolution rate of 526 μmol h^{-1} g^{-1}. The higher photocatalytic activity of AuPd/TiO_2 sample may be attributed to the reason that the interfaces between AuPd and TiO_2 effectively promote the separation efficiency of the photogenerated electron-hole pairs. However, a further increasing of AuPd NPs content leads to a decrease of H_2 evolution activity. This decrease can be related to the increasing in the opacity of the composite samples. The addition of a large amount of dark-brown AuPd can lead to block of the active sites on the surface, and also reduce the intensity of light through the depth of the reaction solution. As a consequence, a suitable content of AuPd NPs is important for regulating the photocatalytic activity of AuPd/TiO_2 nanosheets.

To further investigate the role of bimetallic AuPd alloys in the catalytic process, the photocatalytic process of Au/TiO_2 and Pd/TiO_2 samples were conducted for a comparison. As shown in Fig.6, 1.0 wt% AuPd/TiO_2 show photocatalytic activity with H_2 evolution rate of 247 μmol h^{-1} g^{-1}, which is much higher than that of 1.0 wt% Au/TiO_2 and 1.0 wt% Pd/TiO_2. After the optimization of AuPd contents, the 0.3 wt% AuPd/TiO_2 shows the highest H_2 evolution rate of 526 μmol h^{-1} g^{-1} in all the samples. The results indicate that the AuPd bimetallic alloys play an important role in enhancement of H_2 evolution activity in the AuPd/TiO_2 nanaosheets catalysts.

To verify the stability of 0.3 wt% AuPd/TiO_2 catalysts, the cycling H_2 evolution experiment was

performed. Fig.7 presents the H_2 evolution curve in cycling photocatalytic run. This result shows that there is no obvious decrease of H_2 evolution after irradiation for 32 h, indicating that the AuPd/TiO_2 present photocatalyst keep stable in the catalytic H_2 production process.

3.3. Photocatalytic mechanism discussion

To identify the photocatalytic mechanism, the electron spin resonance (ESR) technique was performed. The ESR technique can be used to detect free radicals in reaction systems. To reveal the main reactive species responsible for the photocatalytic reaction over the AuPd/TiO_2 nanosheets, a series of quenchers were employed to scavenge the relevant reactive species. The DMPO (5, 5-dimethyl-1-dimethy N-oxide) generally used as a radical scavenger owing to the formation of stable free radical, DMPO-O_2^- or DMPO-·OH.

Fig.8(a,b) illustrates ESR spectra measured as the effect of light irradiation over the 0.3 wt% AuPd/TiO_2 nanosheets at room temperature in air. As shown in Fig.8a, there was no ESR signal in the dark, a gradual evolution of ESR peaks for DMPO-O_2^- adducts were observed in methanol under UV light irradiation. Moreover, Fig.8b shows that the signals of DMPO-·OH adducts were detected in water under otherwise identical conditions. When TiO_2 absorbs a photon with energy larger than its band-gap (λ<390 nm), electrons is excited from the valence band (VB) to the conduction band (CB) of TiO_2 to produce electron–hole pairs. Subsequently, the pair is separated into an electron and a hole. The e_{cb}^- and h_{vb}^+ migrate to the surface where they are ultimately captured. The ESR test was operating in the air. That is to say, there has been oxygen in the testing process. The electrons in photocatalysts are good reductants that can easily capture the adsorbed oxygen onto the composite catalyst surface and reduce it to superoxide radical. There is no ESR signal in the dark, a gradual evolution of ESR peaks for DMPO-O_2^- adducts are observed in methanol under UV light irradiation. In the non-vacuum system, the oxygen and hydrogen can easily react to form water, making the test results is not accurate. The gas

chromatography can only detect the hydrogen content in vacuum condition. And then, the electron can also react with H^+ instead of O_2 and cause the formation of hydrogen in the photocatalytic system. As the result, it is indicate that the photo-generated electrons play the predominant role toward the water splitting reaction in anaerobic environment under UV-visible light irradiation.

Based on the above results and the photocatalytic activities of AuPd/TiO_2 nanosheets, a possible mechanism for photocatalytic H_2 evolution over AuPd/TiO_2 catalyst is proposed and illustrated in Fig.9. Under UV-visible light irradiation, ultrathin 2D TiO_2 nanosheets absorbs photons and excites electron-hole pairs. However, the photogenerated electrons and holes are likely to recombine without co-catalyst. The significant enhancement of H_2 evolution can be attributed to synergistic effect between TiO_2 and AuPd alloys. After the AuPd alloys are introduced, the two types of materials closely combine together and form intimate interfaces (Fig.2f). The bimetallic AuPd NPs have higher trapping electron ability and can promote electron transfer from TiO_2 towards AuPd alloys surface due to the lower Fermi level. Therefore, in the AuPd/TiO_2 system, the photogenerated electrons in the CB of the TiO_2 transfer to AuPd co-catalysts via contacting interfaces, making the conduction band electrons more mobile and impelling the separation of electron-hole pairs. The holes in the VB of TiO_2 oxidize the sacrificial agent (methanol) to products, such as CO_2, H_2O et al. Therefore, the recombination process of the electron-hole pairs is effectively inhibited, resulting to obvious improvement of H_2 production for the AuPd/TiO_2 photocatalysts.

In order to confirm the above analysis, it is necessary and important to fully understand the behaviors of charge carriers in AuPd/TiO_2 nanosheets.[42] The SPC technique was conducted to reveal the transfer behaviors of photogenerated electron-hole pairs of AuPd/TiO_2, which could be beneficial for clarifying the influence of bimetallic AuPd alloys. Fig.10 presents the SPC spectra of AuPd/TiO_2 with different bimetallic AuPd contents. The SPC response ranging from 300 nm to 550 nm can be seen for

pure TiO_2 nanosheets. This is typical characteristic of n-type semiconductor in SPC, where positive charges from inner semiconductor migrate to the surface. The intensity of the SPC spectra represents the separation efficiency of photo-induced charge carriers. The 0.1wt% AuPd/TiO_2 sample produces stronger SPC signal in contrast with pure TiO_2 sample, indicating that the photogenerated electron-hole pairs are separated more effectively. The 0.3wt% AuPd/TiO_2 sample shows the highest SPC intensity, indicating the maximal separating efficiency of electron-hole pairs. The SPC signals illustrate that an optimal content of bimetallic AuPd is favor of electron-hole separation in TiO_2 nanosheets. However, if more AuPd NPs are added, the light absorption by TiO_2 reduces as more AuPd NPs prevent the light from reaching the TiO_2 surface, leading to the decrease of SPC signal in comparison to that for 0.3wt% AuPd/TiO_2 sample. It is more important that the SPC spectra are consistent with the results of photocatalytic H_2 evolution, which can understand the origin of enhanced separation efficiency of photogenerated electron-hole pairs in the AuPd/TiO_2 nanosheets.

4. Conclusions

In summary, a novel AuPd/TiO_2 photocatalysts were synthesized via a facile in situ synthesis method. The introducing of bimetallic AuPd species did not affect the morphology and crystal structure of ultrathin 2D TiO_2 nanosheet. The composite photocatalysts exhibited enhanced photocatalytic activity in the presence of AuPd NPs, and the highest efficiency was observed over 0.3 wt% AuPd/TiO_2 sample. The presence of AuPd could increase the interfacial charge transfer and inhibit the recombination of electron-hole pairs. A possible photocatalytic mechanism is proposed based on the experimental results. Therefore, the bimetallic AuPd NPs decorated 2D TiO_2 nanosheet is a promising functional material which can be potentially used for new energy field.

Author information

Corresponding Author

* E-mail: gelei08@sina.com (Professor Lei Ge)

Acknowledgements

This work was financially supported by the National Science Foundation of China (Grant No. 21003157 and 21273285), Beijing Nova Program (Grant No. 2008B76), and Science Foundation of China University of Petroleum, Beijing (Grant No. KYJJ2012-06-20).

References

1 L. Ge, C. C. Han and J. Liu, *App. Catal., B*, 2011, **108-109**, 100-107.

2 Y. H. He, D. Z. Li, J. Chen, Y. Shao, J. J. Xian, X. Z. Zheng and P. Wang, *RSC Adv*., 2014, **4**, 1266-1269.

3 X. Wang, D. P. Liu, S. Y. Song and H. J. Zhang, *J. Am. Chem. Soc*., 2013, **135**, 15864-15872.

4 L. Ge, F. Zuo, J. Liu, Q. Ma, C. Wang, D. Sun, L. Bartels and P. Feng, *J. Phys. Chem. C*, 2012, **116**, 13708−13714.

5 S. Chuangchote, J. Jitputti, T. Sagawa and S. Yoshikawa, *ACS Appl. Mater. Interfaces,* 2009, **1**, 1140-1143.

6 X. B. Chen, S. H. Shen, L. J. Guo and S. S. Mao, *Chem. Rev.*, 2010, **110**, 6503-6570.

7 B. Seger, T. Pedersen, A. B. Laursen, P. C. Vesborg, O. Hansen and I. Chorkendorff, *J. Am. Chem. Soc*., 2013, **135**, 1057-1064.

8 T. Umebayashi, T. Yamaki, S. Tanaka and K. Asai, *Chem. Lett*., 2003, **32**, 330-331.

9 J. C. Zhao, T. X. Wu, K. Q. Wu, K. Oikawa, H. Hidaka and N. Serpone, *Environ. Sci. Technol*., 1998, **32**, 2394-2400.

10 R. Asahi, T. Morikawa, H. Irie and T. Ohwaki, *Chem. Rev*., 2014, **114**, 9824-9852.

11 L. X. Sang, Y. X. Zhao and C. Burda, *Chem. Rev*., 2014, **114**, 9283-9318.

12 V. Subramanian, E. E. Wolf and P. V. Kamat, *Langmuir*, 2003, **19**, 469-474.

13 J. Y. Park, J. R. Renzas, B. B. Hsu and G. A. Somorjai, *J. Phys. Chem. C*., 2007, **111**, 15331-15336.

14 S. Q. Liu, N. Zhang, Z. R. Tang and Y. J. Xu, *ACS Appl. Mater. Interfaces*, 2012, **4**, 6378–6385.

15 X. X. Yao, T. Y. Liu, X. H. Liu and L. L. Lu, *Chem. Eng. J*., 2014, **255**, 28-39.

16 L. Kumaresan, M. Mahalakshmi, M. Palanichamy and V. Murugesan, *Ind. Eng. Chem. Res*., 2010, **49**, 1480–1485.

17 Z. A. Huang, Q. Sun, K. L. Lv, Z. H. Zhang, M. Lia and B. Li, *App. Catal*., *B*, 2015, **164**, 420–427.

18 W. Y. Yao, B. Zhang, C. P. Huang,C. Ma, X. L. Song and Q. J. Xu, *J. Mater. Chem*., 2012, **22**, 4050-4055.

19 J. H. Pan and W. I. Lee, *Chem. Mater.,* 2006, **18**, 847–853.

20 Y. H. Hu, *Angew. Chem. Int. Ed*., 2012, **51**, 12410-12412.

21 G. Liu, L. C. Yin, J. Q. Wang, P. Niu, C. Zhen, Y. P. Xie and H. M. Cheng, *Energy Environ. Sci*., 2012, **5**, 9603-9610.

22 L. Wang and T. Sasaki, *Chem. Rev*., 2014, **114**, 9455–9486.

23 W. G. Tu, Y. Zhou, Q. Liu, Z. Q. Tian, J. Gao, X. Y. Chen, H. T. Zhang, J. G. Liu and Z. G. Zou, *Adv. Funct. Mater*., 2012, **22**, 1215–1221.

24 C. H. Chen, L. S. Sarma, J. M. Chen, S. C. Shih, G. R. Wang, D. G. Liu, M. T. Tang, J. F. Lee and B. J. Hwang, *ACS Nano*, 2007, **1**, 114–125.

25 M. L. Wu, D. H. Chen and T. C. Huang, *J. Colloid Interface Sci*., 2001, **243**, 102–108.

26 N. Toshima and Y. Wang, *Langmuir*, 1994, **10**, 4574–4580.

27 D. Cakir and O. Gulseren, *J. Phys. Chem. C*, 2012, **116**, 5735-5746.

28 C. G. Raab and J. A. Lercher, *Catal. Lett.*, 1993, **18**, 99-109.

29 L. Dalannoy, G. Thrimurthulu, P. S. Reddy, C. Methivier, J. Nelayah, B. M. Reddy, C. Ricolleau and C. Louis, *Phys. Chem. Chem. Phys*., 2014, **16**, 26514-26527.

30 C. Kong, S. X. Min and G. X. Lu, *Chem. Commun*., 2014, **50**, 9281-9283.

31 M. Bonarowska, J. Pielaszek, W. Juszczyk and Z. Karpinski, *J. Catal*., 2000, **195**, 304-315.

32 A. M. Venezia, V. L. Parola, G. Deganello, B. Pawlec, J.L.G. Fierro, *J. Catal*., 2003, **215**, 317-325.

33 A. M. Venezia, V. La Parola, V. Nicoli and G. Deganello, *J. Catal*., 2002, **212**, 56-62.

34 P. Landon, P.J. Collier, A. J. Papworth, C. J. Kiely and G. J. Hutchings, *Chem. Commun*., 2002, **18**, 2058-2052.

35Z. Q. Sun, T. Liao, Y. H. Dou, S. M. Hwang, M. S. Park, L. Jiang, J. K. Kim and S. X. Dou, *Nature Communications*, 2014, **5**, 553-558.

36 R. Su, R. Tiruvalam, A. J. Logsdail, Q. He, C. A. Downing, M. T. Jensen, N. Dimitratos, L. Kesavan, P. P. Wells, R. Bechstein, H. H. Jensen, S. Wendt, C. R. A. Catlow, C. J. Kiely, G. J. Hutchings and F. Besenbacher, *ACS Nano*, 2014, **8**, 3490-3497.

37 T. Q. Li, H. H. Zhou, J. Q. Huang, J. L. Yin, Z. X. Chen, D. Liu, N. S. Zhang and Y. F. Kuang, *Colloids Surf., B*, 2014, **463**, 55-62.

38 Y. C. Zhang, J. Li and H. Y. Xu, *Appl. Catal., B*., 2012, **123-124**, 18-26.

39 S. Wendt, P. T. Sprunger, E. Lira, G. K. H. Madsen, Z. S. Li, J. Hansen, J. Matthiesen, A. B. Rasmussen, E. Lagsgaard, B. Hammer and F. Besenbacher, *Science*, 2008, **320**, 1755–1759.

40 A. Cybula, J. B. Priebe, M. M. Pohl, J. W. Sobczak, M. Schneider and A. Z. Jurek, *Appl. Catal., B*, 2014, **152-153**, 202-211.

41 A. Murugadoss, K. Okumura and H. Sakurai, *J. Phys. Chem. C,* 2012, **116**, 26776−26783

42 M. Yang, D. J. Wang, L. Peng, Q. D. Zhao, Y. H. Lin and X. Wei, *Sens. Actuators, A*, 2006, **117**,

80-85.

Figure Captions:

Fig.1 XRD patterns of AuPd/TiO_2 composite photocatalysts.

Fig.2 TEM images (a, b, d, e) and HRTEM images (c, f) of ultrathin 2D TiO_2 nanosheets (a–c) and AuPd/TiO_2 composite (d-f).

Fig.3 DRS spectra of the AuPd/TiO_2 composite samples with different AuPd alloy NPs contents.

Fig.4 XPS spectra of 1.0 wt% AuPd/TiO_2 sample: (a) O 1s; (b) Ti 2p; (c) Au 4f; (d) Pd 3d.

Fig.5 Photocatalytic H_2 evolution over AuPd/TiO_2 composite samples with different AuPd NPs contents under UV-visible light: 0 wt% AuPd, 0.1 wt% AuPd, 0.3 wt% AuPd, 0.5wt % AuPd, 1.0 wt% AuPd.

Fig.6 Rate of H_2 evolution over AuPd/TiO_2 composite samples with different AuPd contents, Pd/TiO_2 and Au/TiO_2 under UV-visible light: (a) 0 wt% AuPd; (b) 1.0 wt% Au; (c) 1.0 wt% Pd; (d) 1.0 wt% AuPd; (e) 0.5 wt% AuPd; (f) 0.3 wt% AuPd; (g) 0.1 wt% AuPd.

Fig.7 Cycling runs for the photocatalytic H_2 evolution in the presence of 0.3 wt% AuPd/TiO_2 composite sample under UV-visible light irradiation.

Fig.8 ESR spectra of AuPd/TiO_2 photocatalysts: (a) O_2^- detected in methanol; (b) •OH detected in water.

Fig.9 The schematic illustration of the proposed mechanism for charge transfer and H_2 evolution in AuPd/TiO_2 composite under UV-visible light irradiation.

Fig.10 SPC spectra of AuPd/TiO_2 photocatalyst with different AuPd alloy NPs contents.

1. 1.

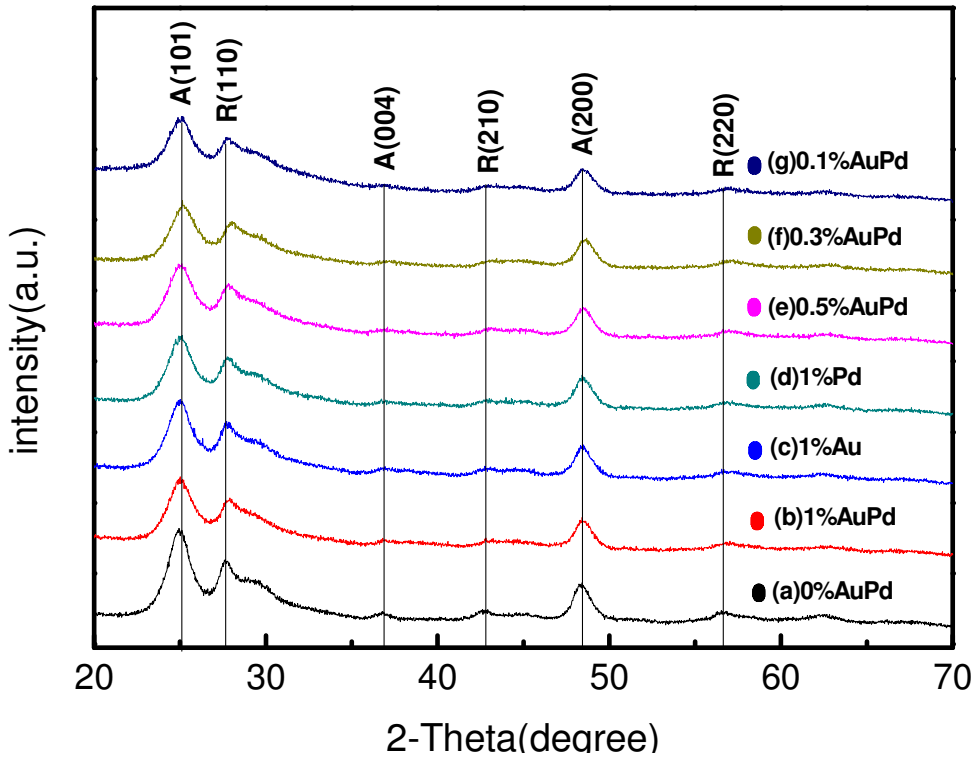

2

3 2.

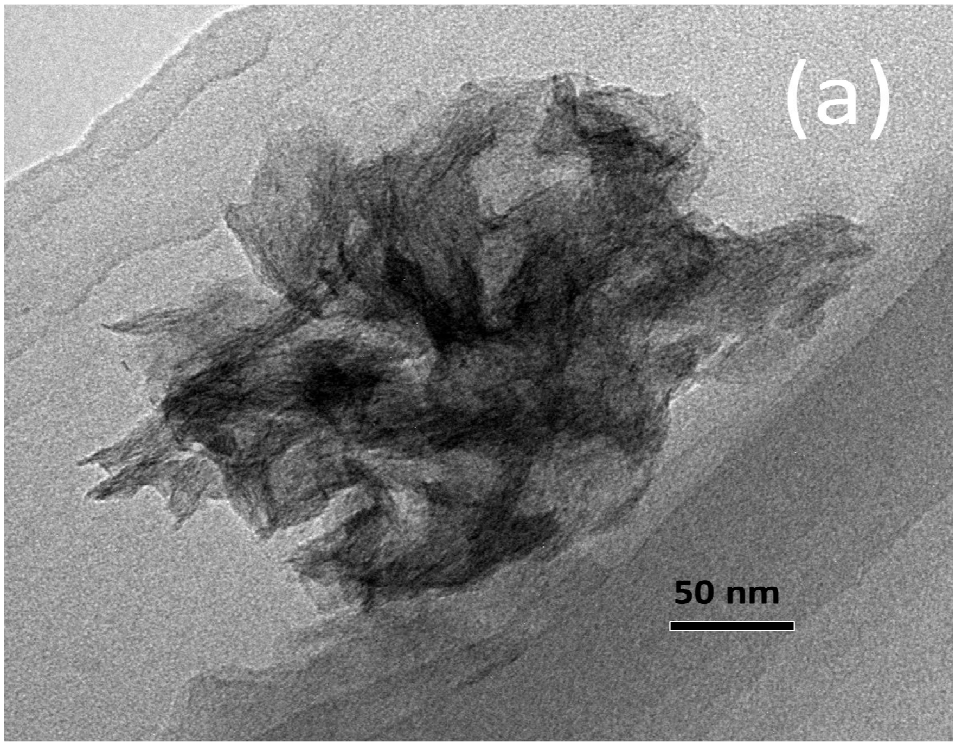

4

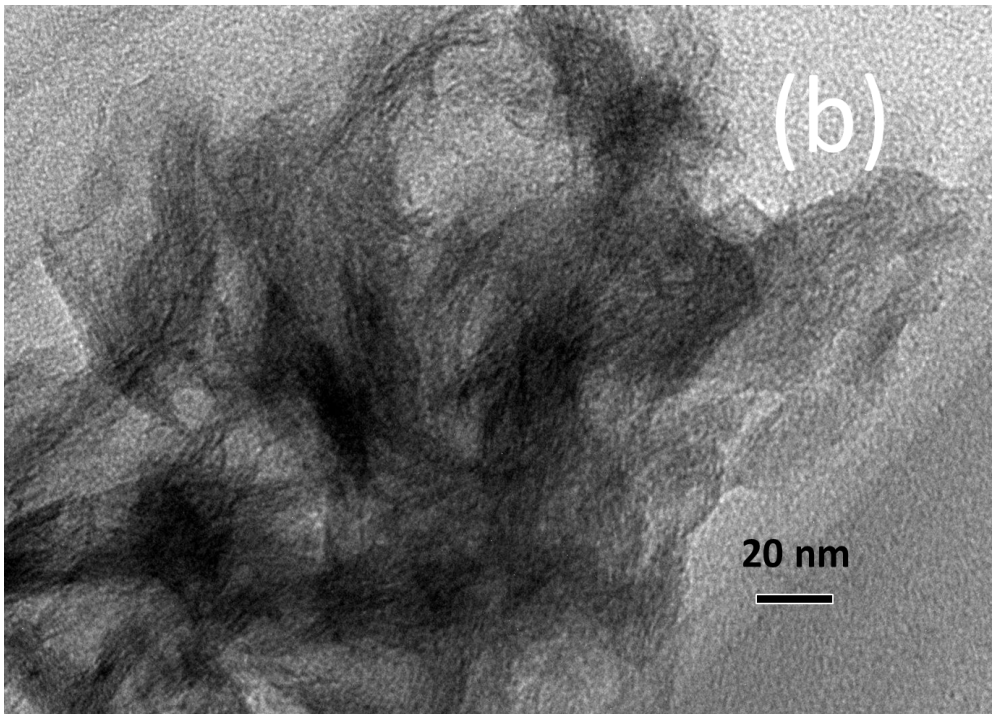

1

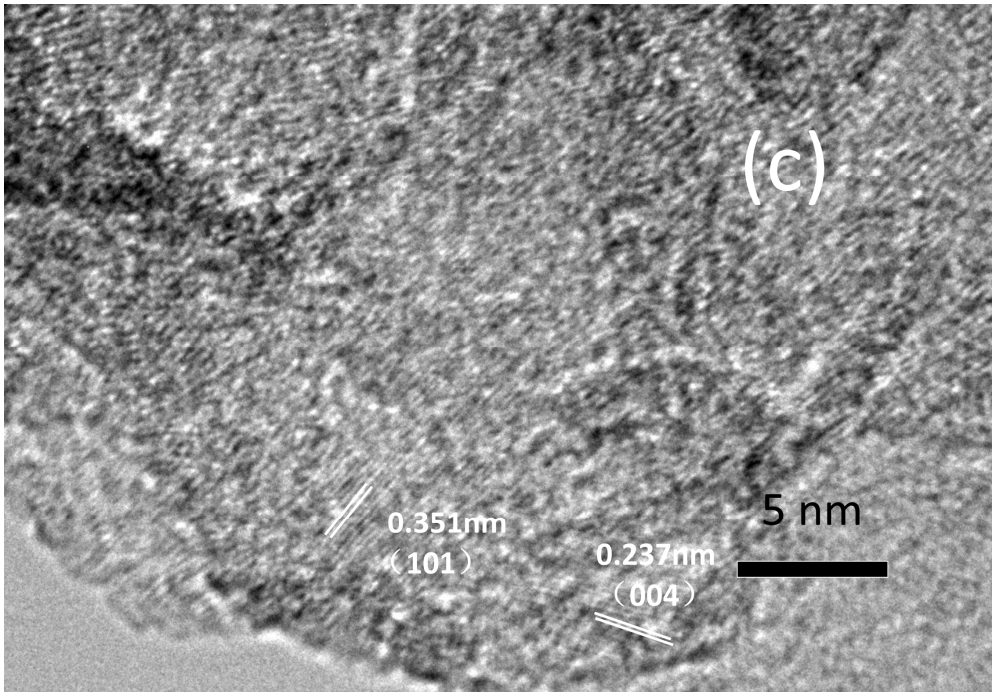

2

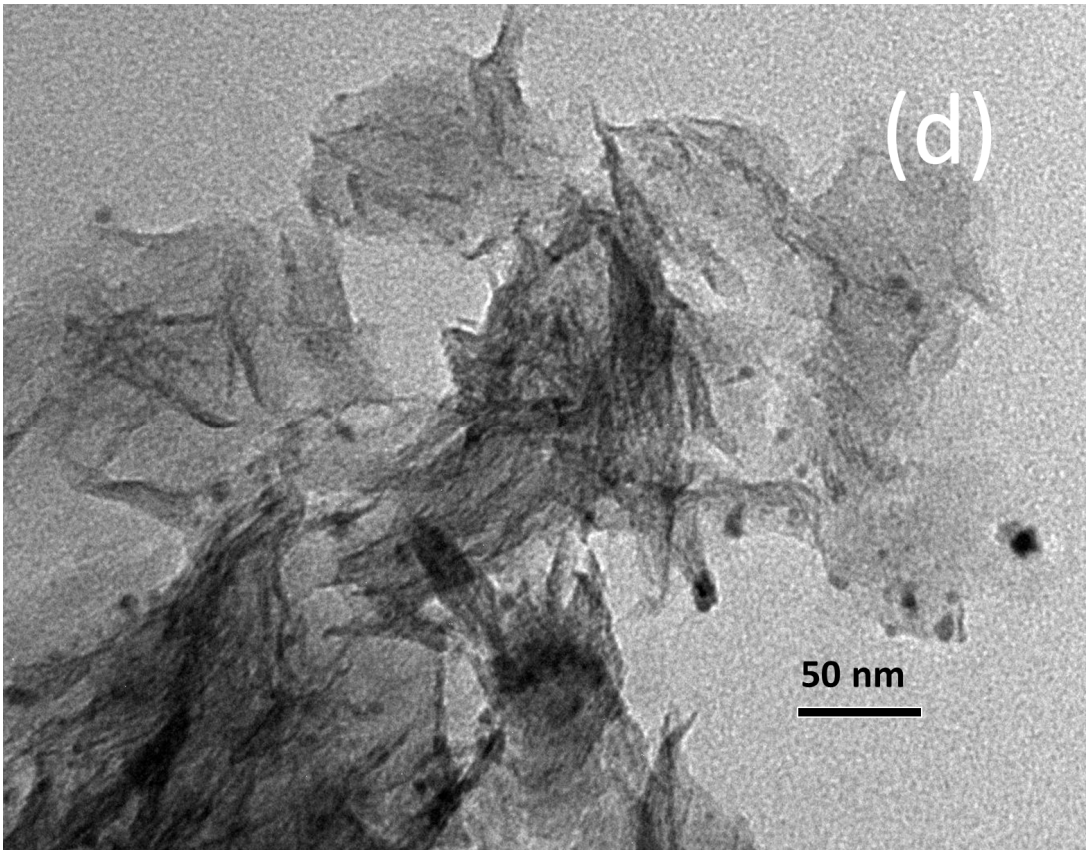

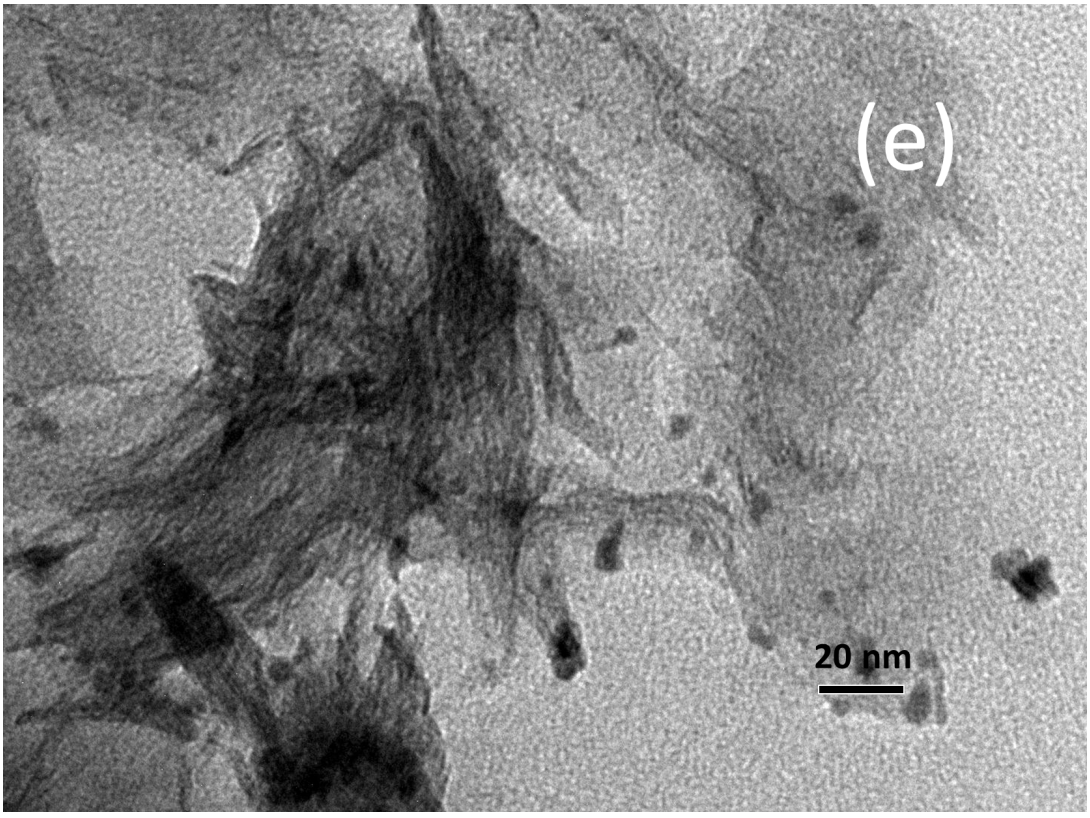

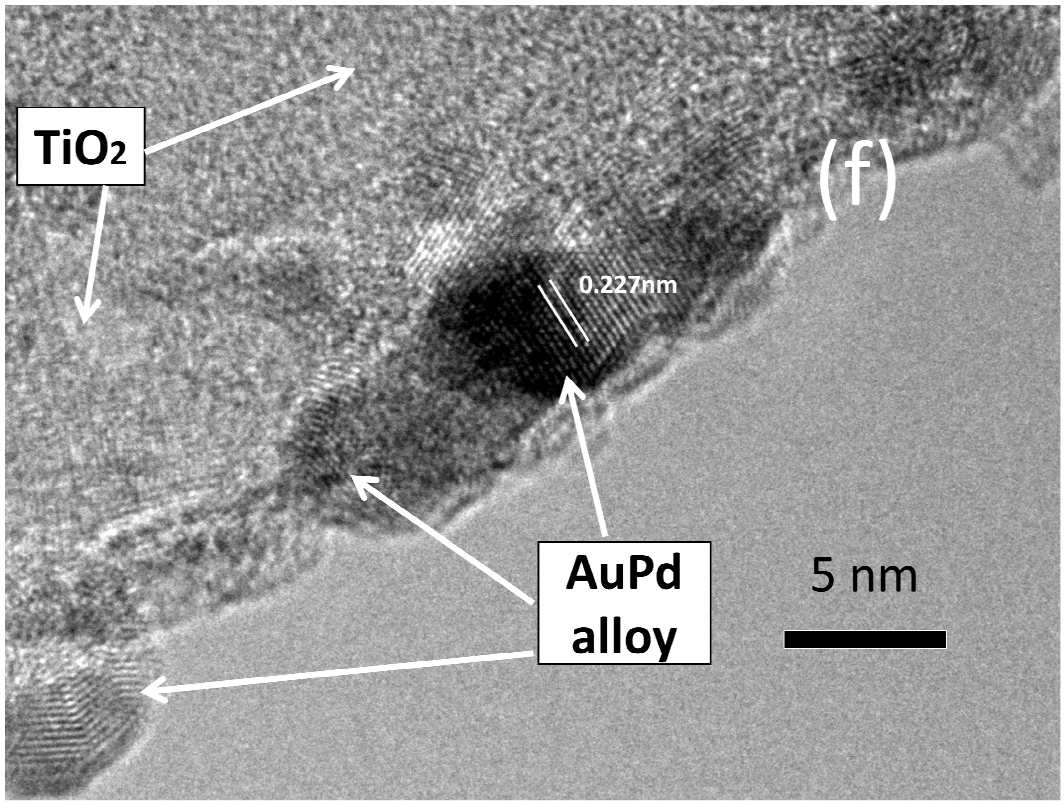

3.

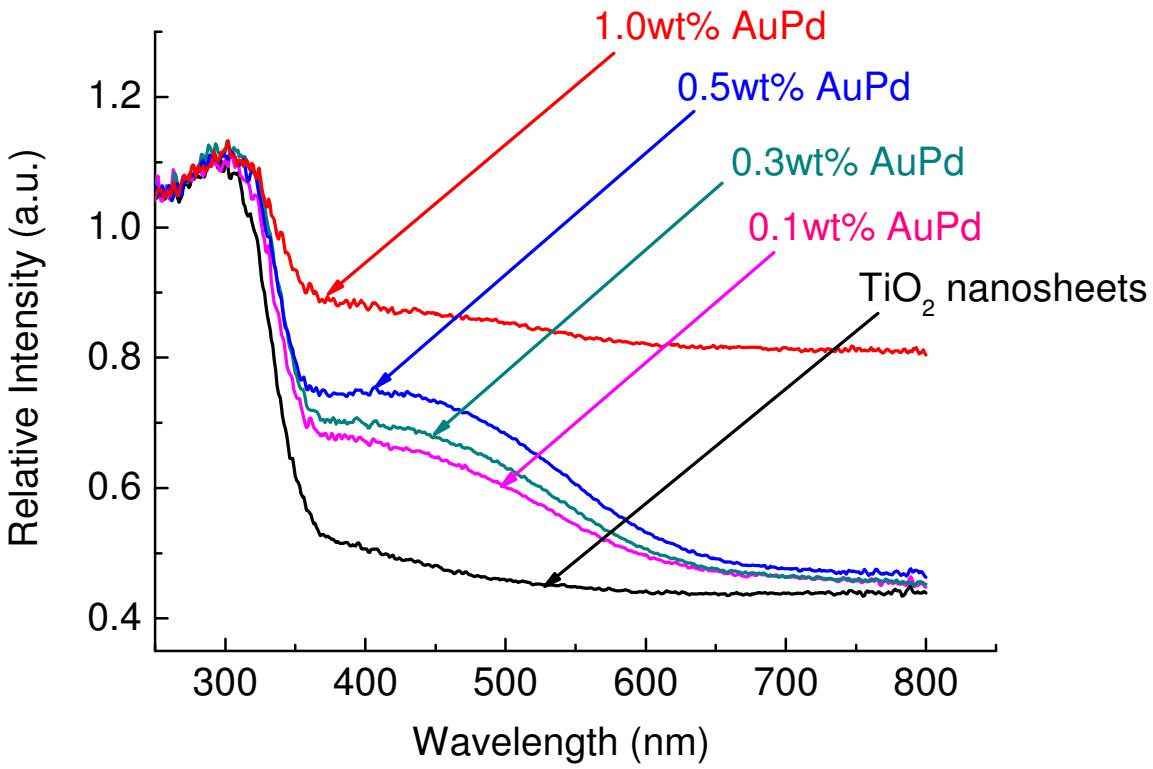

4.

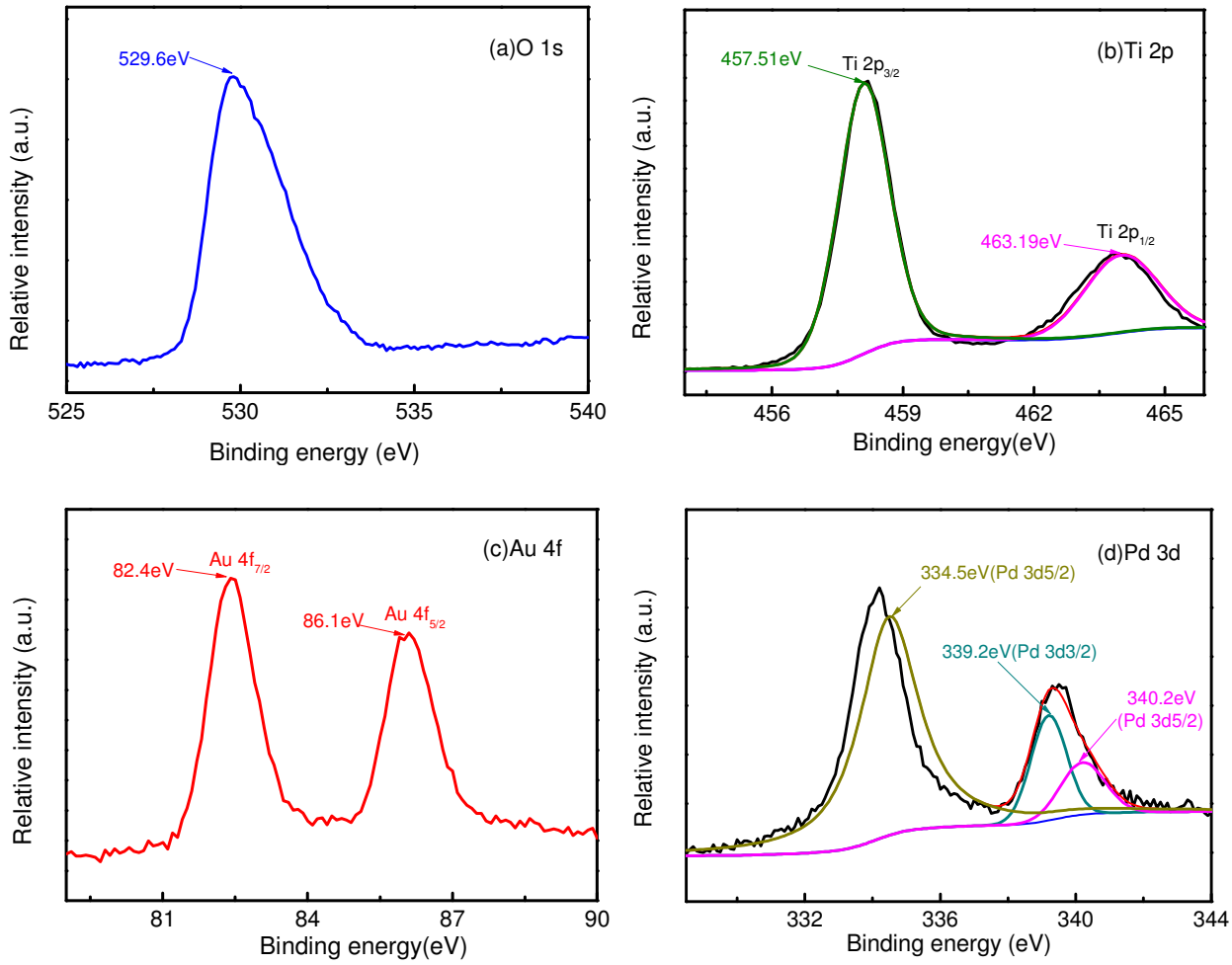

5.

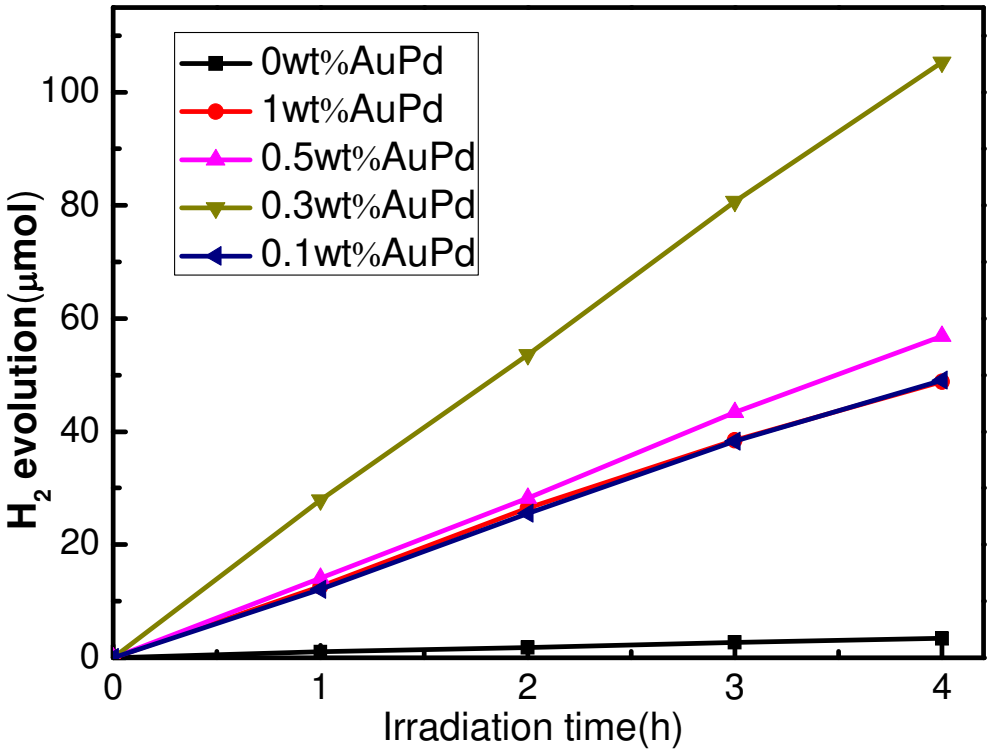

6.

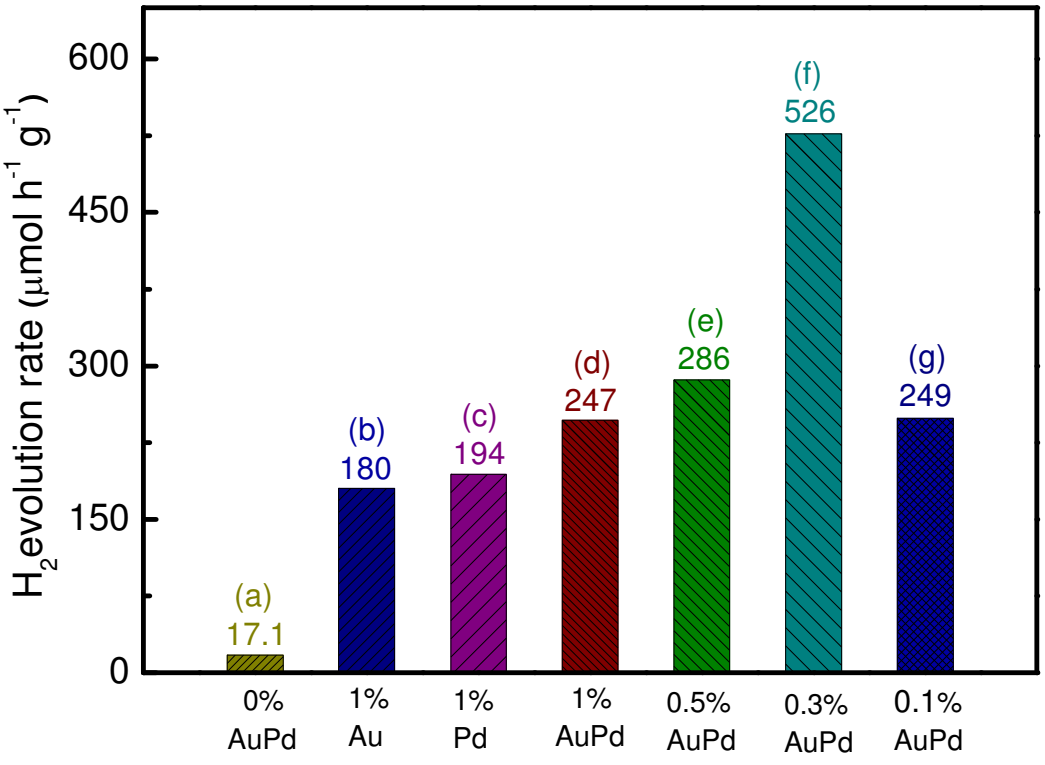

7.

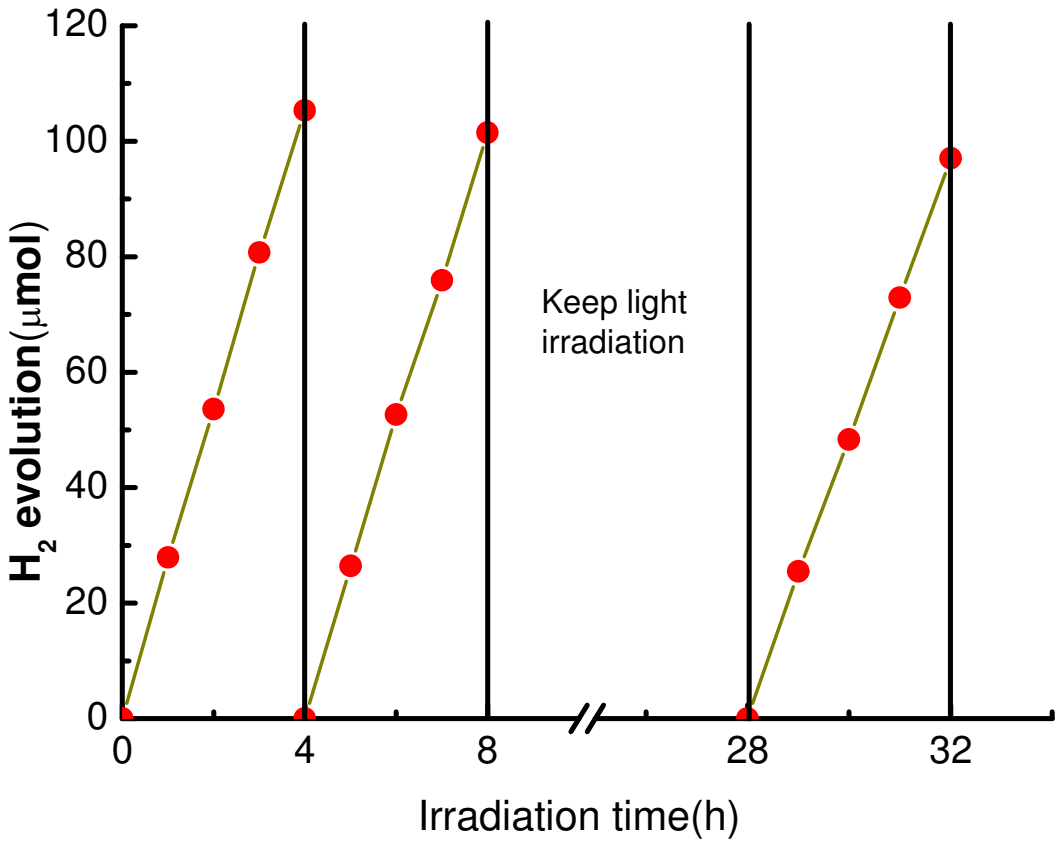

8.

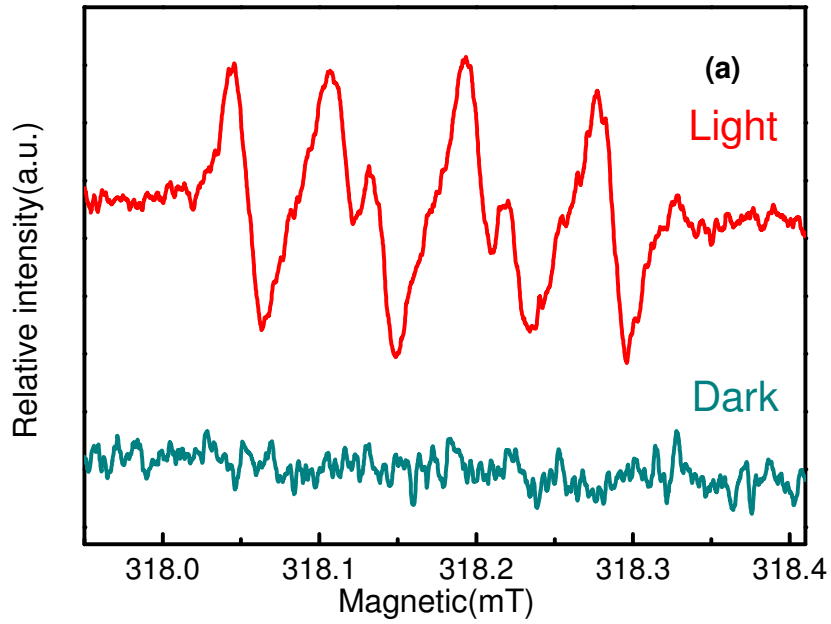

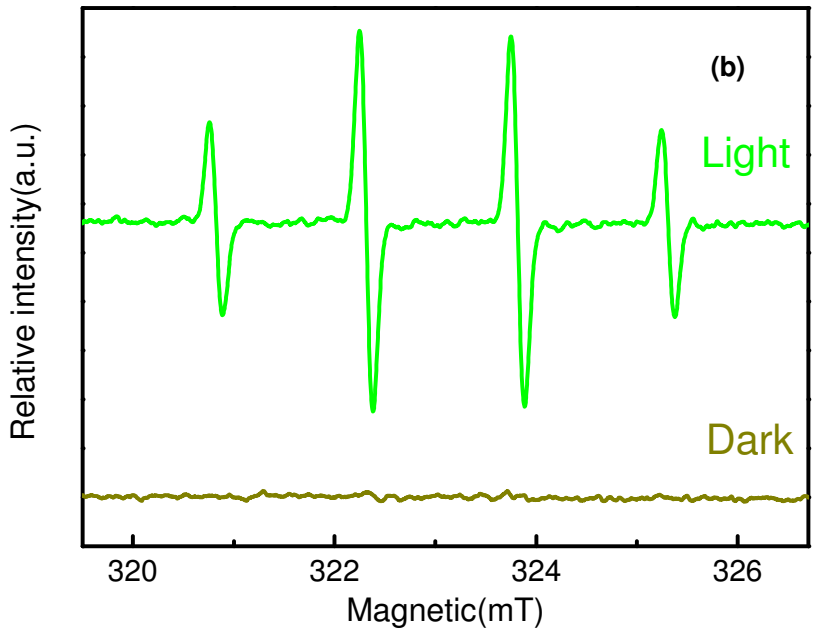

9.

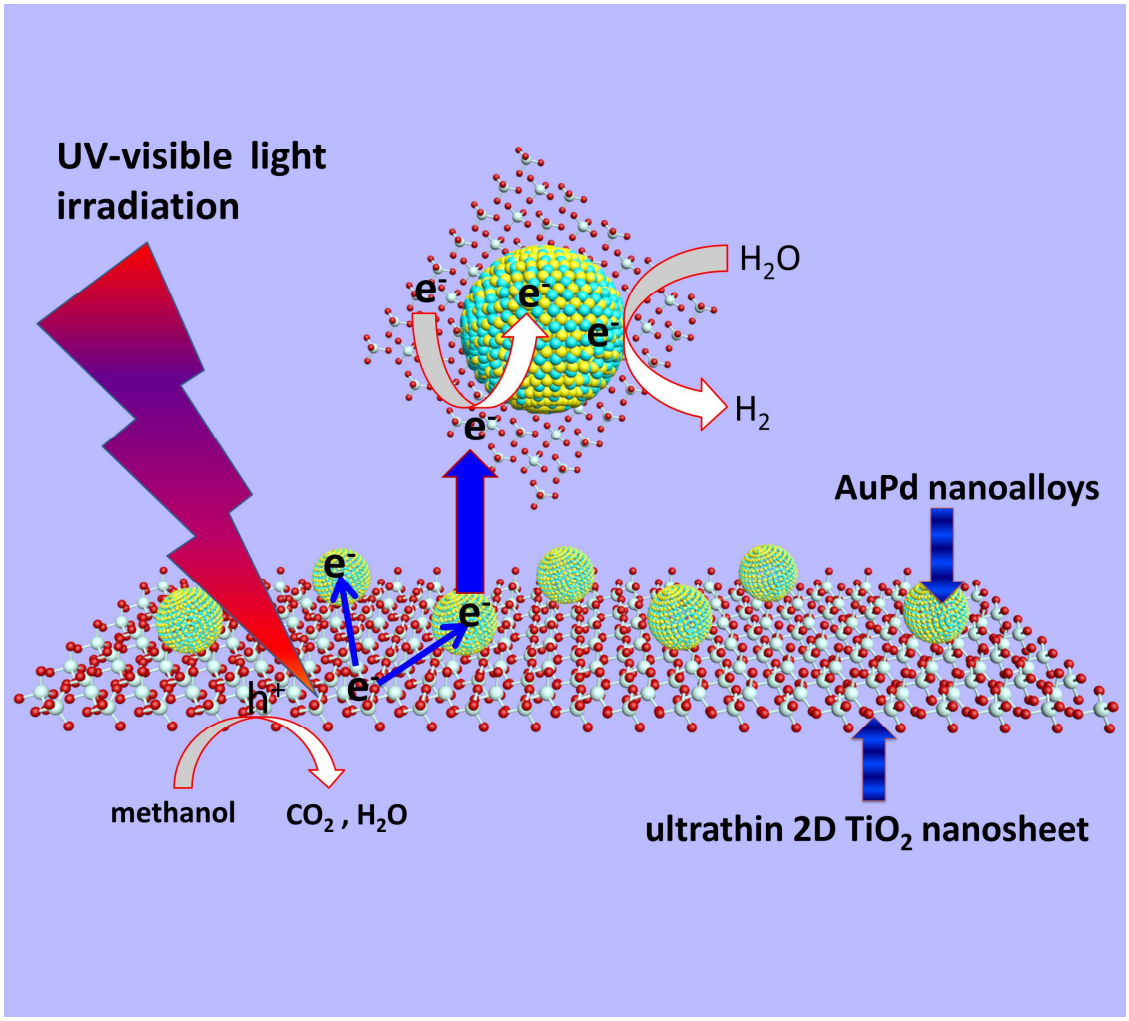

10.

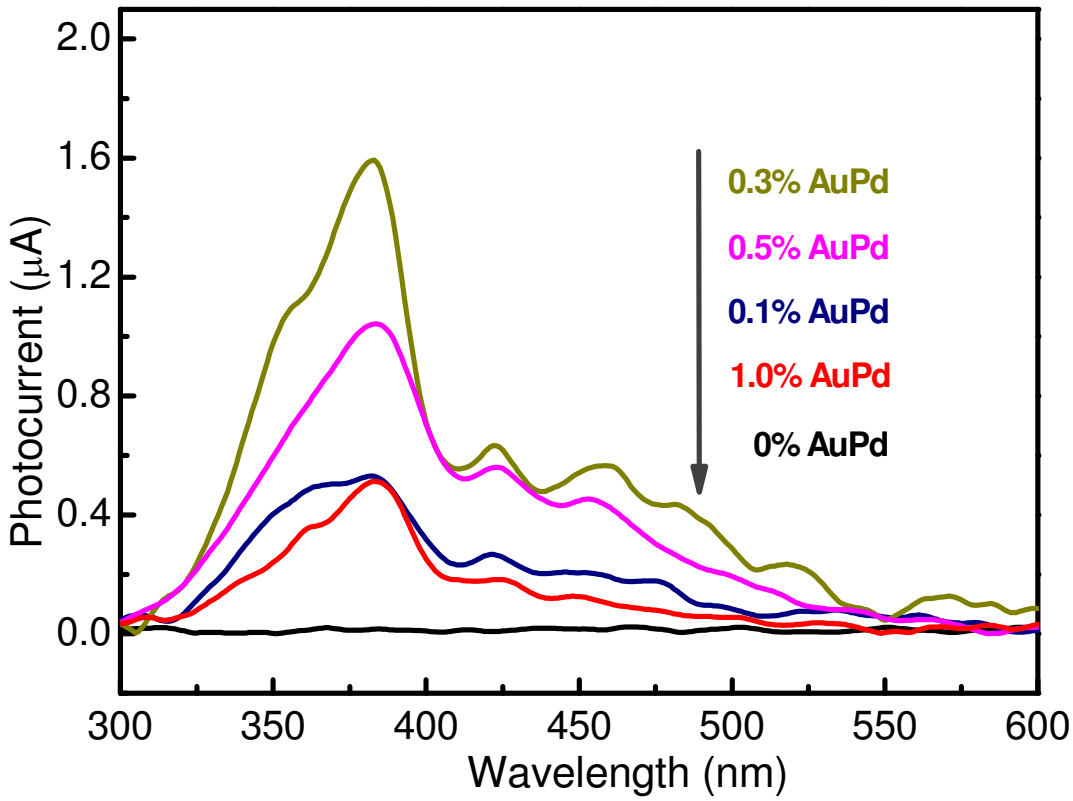

Graphical Abstract